The Astrophysical Journal, 645:1092–1101, 2006 July 10

SPITZER OBSERVATIONS OF THE DUSTY WARPED DISK OF CENTAURUS A

Alice C. Quillen
Department of Physics and Astronomy, University of Rochester,
Rochester, NY 14627; aquillen@pas.rochester.edu

and

Mairi H. Brookes, Jocelyn Keene, Daniel Stern, Charles R. Lawrence, and Michael W. Werner
Jet Propulsion Laboratory, California Institute of Technology, 4800 Oak Grove Drive, Pasadena, CA 91109;
Mairi.H.Brookes@jpl.nasa.gov, jkeene@caltech.edu, stern@zwolfkinder.jpl.nasa.gov,
charles.lawrence@jpl.nasa.gov, Michael.W.Werner@jpl.nasa.gov
Received 2006 January 6; accepted 2006 March 17

ABSTRACT

Spitzer mid-infrared images of the dusty warped disk in the galaxy Centaurus A show a parallelogram-shaped structure. We successfully model the observed mid-infrared morphology by integrating the light from an emitting, thin, and warped disk, similar to that inferred from previous kinematic studies. The models with the best match to the morphology lack dust emission within the inner 0.1–0.8 kpc, suggesting that energetic processes near the nucleus have disturbed the inner molecular disk, creating a gap in the molecular gas distribution.

Subject headings: galaxies: individual (NGC 5128) — galaxies: ISM — galaxies: peculiar — galaxies: structure

Online material: color figures

1. INTRODUCTION

Centaurus A (NGC 5128) is the nearest of all the giant radio galaxies. Because of the disk of gas and dust in its central regions, Cen A is suspected to be the product of a merger of a small gas-rich spiral galaxy with a larger elliptical galaxy (Baade & Minkowski 1954). Numerical simulations of such mergers predict large shell-like features (Hernquist & Quinn 1988) that have been observed in Cen A over a large range of radii (Malin et al. 1983; Peng et al. 2002). Some features contain atomic and molecular gas, implying that they were formed from material stripped from a galaxy relatively recently, fewer than a few galactic rotation periods ago (Schiminovich et al. 1994; Charmandaris et al. 2000). Tidal features associated with this debris have also been identified, supporting the relatively short (a few times 10^8 yr) estimated timescale since the merger took place (Peng et al. 2002).

In its central regions, NGC 5128 exhibits a well-recognized, optically dark band of absorption across its nucleus. This dusty disk was first modeled as a transient warped structure by Tubbs (1980). Bland (1986), Bland et al. (1987), Nicholson et al. (1992), and Quillen et al. (1992) found that the kinematics of the ionized and molecular gas are well modeled by a warped disk composed of a series of inclined connected rings undergoing circular motion (as also explored for other galaxies with peculiar morphology by Steiman-Cameron et al. 1992). The model explored by Quillen et al. (1993) modified the kinematic model by Quillen et al. (1992) to fit the morphology of the absorptive, dusty disk seen in near-infrared images and proposed a timescale of about 200 million yr since the core of an infalling spiral galaxy reached and merged with the elliptical galaxy nucleus. An initially flat disk, misaligned with the galaxy principal symmetry axis, becomes increasingly corrugated as a function of time. The short timescale estimated since the merger in NGC 5128 is approximately consistent with the timescale suggested by the presence of tidal debris and by the shell-like features containing atomic hydrogen (Schiminovich et al. 1994; Peng et al. 2002) and molecular gas (Charmandaris et al. 2000). An alternative model accounting for the warped disk is the polar ring model by Sparke (1996), which is consistent with the polar orbit of the disk implied by the galaxy isophotes in the outer galaxy (Malin et al. 1983; Haynes et al. 1983; Peng et al. 2002) but requires a longer timescale to account for the twist of the warp.

More recent observations of the central region include submillimeter imaging with the Submillimeter Common User Bolometer Array (SCUBA) and mid-infrared imaging with the Infrared Camera (ISOCAM) on the *Infrared Space Observatory* (*ISO*) satellite (Mirabel et al. 1999; Leeuw et al. 2002). At these wavelengths, the dusty disk is seen in emission rather than in absorption. At 100–200 pc from the nucleus, the galaxy contains a molecular circumnuclear disk that has been studied in molecular line emission (Israel et al. 1990, 1991) and has been resolved in Paα emission (Schreier et al. 1996; Marconi et al. 2001). For a recent summary of the wealth of observational studies carried out on this peculiar and active nearby galaxy, see the comprehensive review by Israel (1998). On the basis of the discussion by Israel (1998), we adopt a distance to Cen A of 3.4 Mpc. At this distance, $1'$ on the sky corresponds to $\approx$1 kpc.

In this manuscript we focus on the geometry of the dusty disk in Cen A as seen from *Spitzer* Infrared Array Camera (IRAC) images. These images are more than 10 times deeper and at twice the angular resolution of previous mid-infrared images of this galaxy (those by Mirabel et al. 1999). Observations are described in § 2. Our geometric model is described in § 3. A discussion and summary follow in § 4.

2. OBSERVATIONS

Figures 1 and 2 present images of NGC 5128 taken on 2004 February 10 in the 3.6, 4.5, 5.8, and 8.0 μm broadband filters (channels 1–4) of the *Spitzer* Infrared Array Camera (Fazio et al. 2004). In each filter, the fixed cluster observing mode was used for these observations to produce a map of 5×6 points, at which five dithered exposures were taken. The exposure time per frame was 12 s. Additional shorter exposures, with 0.4 s frames, were also taken to correct for possible saturation in the longer exposure frames. The coverage of the map at each position on the sky

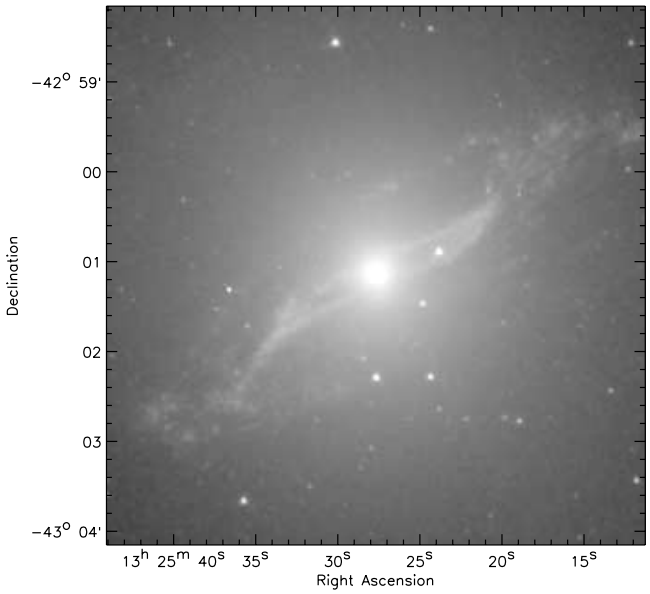

FIG. 1.— Central region of Cen A at 3.6 μm, taken with the IRAC camera on board the *Spitzer Space Telescope*. The emission is shown on a logarithmic scale. At 3.6 and 4.5 μm, starlight is seen in addition to emission from dust. At longer wavelengths, emission from dust is primarily seen. North is up, and east is to the left.

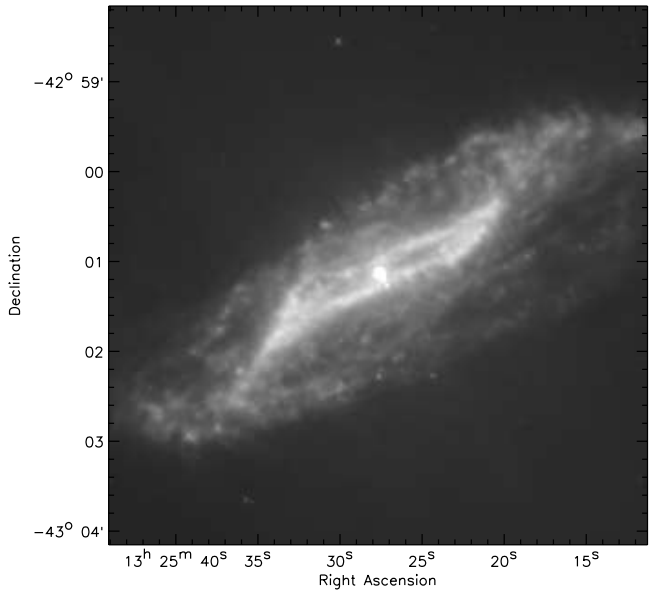

FIG. 2.—Same as Fig. 1, but for an IRAC image at 8.0 μm. This figure is shown on a logarithmic scale. [*See the electronic edition of the Journal for a color composite version of this figure*.]

varies between 3 and 10 frames, with an average coverage of 6 frames, corresponding to an exposure time of 72 s.

Before mosaicking, the basic calibrated data (BCD) frames were corrected for artifacts using the IRAC artifact mitigation code (excluding the pull-down correction) available from the *Spitzer* Science Center's contributed software pages.[1] The final mosaicked images were produced from the dithered frames by applying the MOPEX software[2] to the corrected BCD frames.

Here we focus on the central $5' \times 5'$ region in the final mosaics. The mosaicked images provide a plate scale with 1.″2 pixels; FWHMs of the point-spread functions are 1.″7, 1.″7, 1.″9, and 2.″0 in channels 1, 2, 3, and 4, respectively. The rms noise levels in these images are 0.025, 0.024, 0.070, and 0.060 MJy sr^{-1} in channels 1, 2, 3, and 4, respectively. The above sensitivities agree with the predictions of the SENS-PET sensitivity estimator in the longer wavelength channels. The 3.6 μm channel contains emission from the stellar component of the galaxy that extends over a large portion of the field of view. This makes the 3.6 μm image about half as sensitive as the SENS-PET prediction for the dust emission.

The IRAC images have about twice the angular resolution and are about 20–100 times deeper than the ISOCAM images (Mirabel et al. 1999). In the inner few arcminutes, the IRAC images exhibit a parallelogram shape in emission (see Figs. 2 and 3*c*). This shape, seen at lower angular resolution, was previously interpreted as an S shape, possibly associated with shocks (Mirabel et al. 1999; Leeuw et al. 2002). A parallelogram morphology has been seen previously in other galaxies. For example, dust absorption features in the SO galaxy NGC 4753 exhibit a parallelogram shape and have been modeled with a warped twisted disk by Steiman-Cameron et al. (1992). When an optically thin warped disk is seen in emission, the edges of folds in the disk correspond to regions of higher surface brightness. Multiple folds are seen along the line of sight (e.g., Bland 1986; Bland et al. 1987; Nicholson et al. 1992; Quillen et al. 1993), implying that some parts of the disk are seen through other parts of the disk. In this case, the morphology would not be nearly symmetric across the origin ($r \rightarrow -r$), as observed, unless the outer disk was nearly optically thin in the mid-infrared. We infer that the disk probably has a low normal optical depth in the mid-infrared (if observed face-on), although the bright edges of the folds and individual clumps in the disk may not be optically thin. The parallelogram is present in all four IRAC bands, although it is most prominent compared to the diffuse emission from starlight in the longer wavelength 5.8 and 8 μm bands.

In visible or near-infrared bands, folds can correspond to regions where absorption from dust obscures background starlight. Folds that are closer to the observer absorb more background starlight from the galaxy. Some of the features seen in emission in the IRAC images coincide with absorption bands previously seen in near-infrared images. Figures 3*a* and 3*b* show a $J - H$ color map made from Two Micron All Sky Survey (2MASS) images from the 2MASS Large Galaxy Atlas (Jarrett et al. 2003) and the 8.0 μm IRAC image overlaid as contours on top of the *J*-band 2MASS image, respectively. We refer here to two shapes, an inner parallelogram and an outer oval. See Figure 3*c* for an outline of these shapes on the 8.0 μm image. The southeastern edge of the parallelogram in the IRAC images lies in the same location as the absorption band $\sim$10″ to the southeast of the nucleus prominent in the near-infrared images. This is consistent with the study by Leeuw et al. (2002), who compared submillimeter images to a visible-band image (also see Fig. 1 by Mirabel et al. 1999). The edge of emission $\sim$1′ to the north of the nucleus (at a surface brightness below that of the parallelogram) in the 8.0 μm IRAC image corresponds to the top of the dust lane prominent in optical images of the galaxy. This corresponds to the extinction feature in the near-infrared color map to the north of the nucleus. Comparing the IRAC images to the 2MASS images, we infer that the southern side of the parallelogram is closer to the observer than the northern side. Because the dust on this side lies in front of the plane perpendicular to the line of sight containing the galaxy nucleus, it absorbs more background starlight and so causes a deeper band of extinction in the near-infrared images.

[1] See http://ssc.spitzer.caltech.edu/archanaly/contributed/browse.html.
[2] Available at http://ssc.spitzer.caltech.edu/postbcd/.

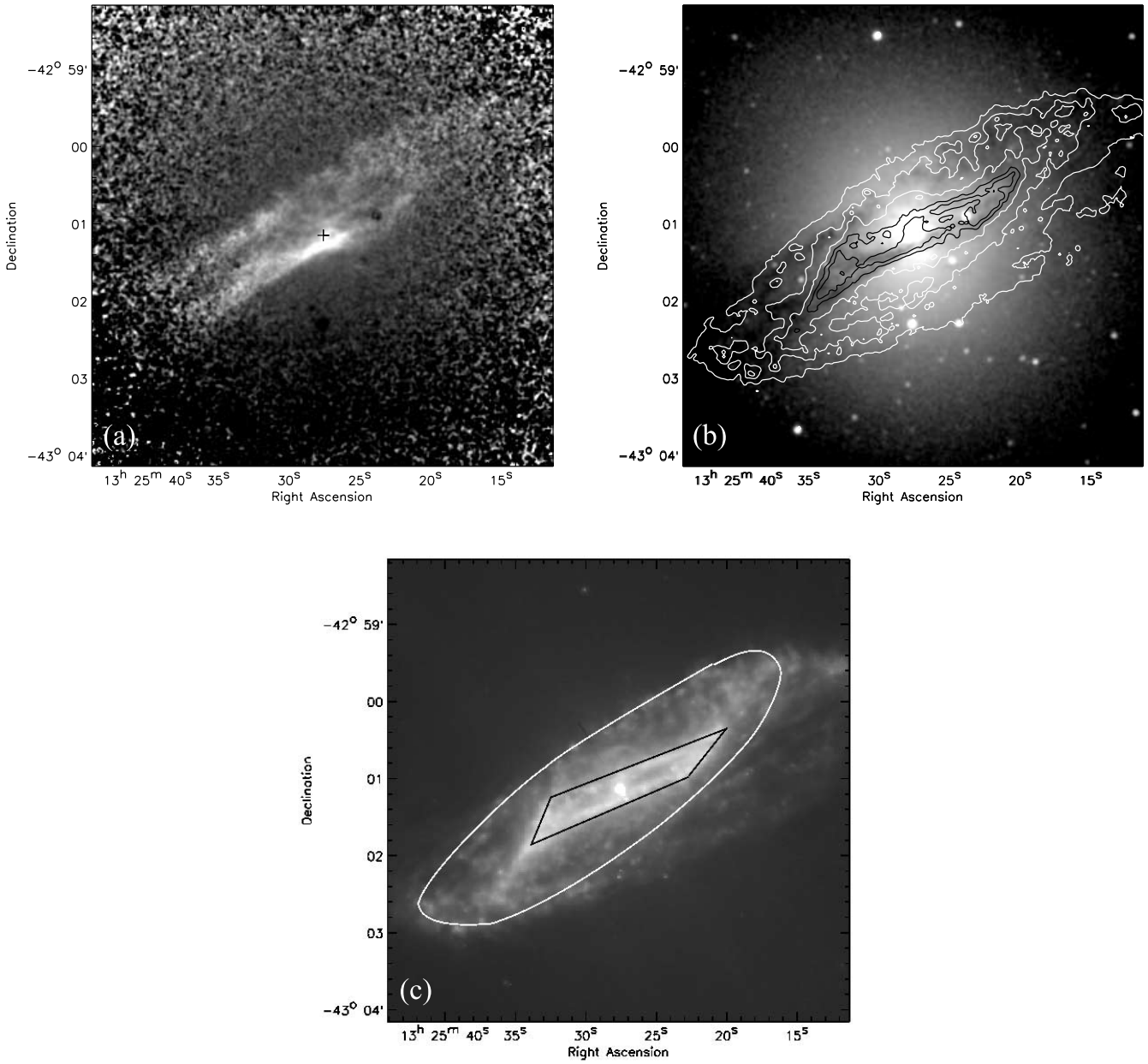

FIG. 3.—(*a*) Color map showing the logarithm of the *H*-band images divided by the *J*-band 2MASS images from Jarrett et al. (2003). Lighter shading corresponds to regions of heavier extinction. Folds in the disk both nearer to and more distant from the observer are seen in the mid-infrared images. However, folds nearer the observer absorb more background starlight and so are more prominent in the near-infrared images. (*b*) *J*-band 2MASS image with 8.0 μm contours overlaid. (*c*) In the text we refer to an outer oval and a parallelogram. This image outlines the two geometric objects on top of the 8.0 μm IRAC image. [*See the electronic edition of the Journal for a color version of this figure*.]

The northern side of the parallelogram lies on the opposite side and so is not seen in the near-infrared images. Likewise, the oval edge of emission $\sim 1'$ to the north of the galaxy nucleus is nearer the observer than that on the opposite edge $\sim 1'$ to the south of the nucleus, and only the northern side causes an absorption feature in the near-infrared images and color maps (see Fig. 3).

3. MODELING OF THE WARPED DISK

At many observed wavelengths, the morphology of Cen A is well reproduced by geometric models of a warped disk (Bland 1986; Bland et al. 1987; Nicholson et al. 1992; Quillen et al. 1992, 1993; Sparke 1996). We describe and extend such modeling here.

A warped disk can be described as a series of tilted rings, each with a different radius *r*. We assume that the gas and dust are evenly distributed on each ring and that each ring is smoothly connected to those at larger and smaller radii. We follow the notation and framework used by Quillen et al. (1992, 1993) to describe the geometry of a warped disk. Each ring is described by two angles, a precession angle, $\alpha(r)$, and an inclination angle, $\omega(r)$. These angles are given with respect to an assumed principal axis of the underlying elliptical galaxy. This axis requires two angles to describe: χ, corresponding to the position angle counterclockwise from north of the axis on the sky, and an inclination angle, ϑ, that describes the tilt of this galactic axis with respect to the line of sight (see Fig. 6 by Quillen et al. 1993). We assume that the galaxy is axisymmetric and not triaxial, so a third angle is not required to describe its orientation. We also assume that the galaxy shape is fixed and not tumbling. Quillen et al.

(1992, 1993) treated the principal axis inclination angle, ϑ, as a free parameter and used the *K*-band isophotal major axis to constrain the other angle, χ.

Our description for the ring projection angles can be related to those of previous works. While Quillen et al. (1992, 1993) described the angles of the warped disk with respect to the principal axis of the underlying elliptical galaxy, Bland et al. (1987) and Nicholson et al. (1992) matched the Hα velocity field with a tilted ring model that described the orientation of the rings with respect to the line of sight. This model fitted the velocity field by adjusting the ring inclination as a function of radius, $i(r)$, and the position angle counterclockwise from north, $p(r)$.

To produce a model image of the mid-infrared emission, we must consider all emitting and absorbing regions along the line of sight at each position on the sky. This is much simpler when the system is optically thin. In this case, we sum all emission along the line of sight at each position on the sky. The near-symmetry of the disk suggests that we can use an optically thin approximation to model this disk. While individual clouds could contain optically thick regions, the bulk of the emitted mid-infrared light is likely to reach the observer. When the disk is optically thin, brighter areas correspond to regions that appear folded from the perspective of the viewer. Here we neglect emission from a spherical component associated with the stars and only consider emission from a thin but warped disk.

Our numerical procedure begins by randomly sampling (x, y) positions in the plane perpendicular to the principal axis of the elliptical galaxy. At each position we compute a z-coordinate based on a smooth (spline) function for the disk precession and inclination angles, $\alpha(r)$ and $\omega(r)$. The points that specify these spline functions are listed in Table 1. The coordinates for each point are then rotated into the viewer's frame. Points along each line of sight are summed to produce a model image. For the functions $\alpha(r)$ and $\omega(r)$, we began with those from Quillen et al. (1993) and slightly varied the angles at different radii to achieve a better match to the observed morphology. Matching was done by visual comparison to the IRAC images. No minimizing fit to the image data values was done. Our procedure is adequate to understand the projection affects associated with an emitting warped disk. Future and more intensive modeling would be required to do a multidimensional and multiwavelength fit. We chose 10 points to describe the spline function for $\alpha(r)$, as this function is rapidly varying with radius. The inclination angle, $\omega(r)$, is only slowly varying, so fewer points were specified. The use of four points allowed us to explore functions with differing curvature.

To construct a model, we must consider the thickness of the disk and its brightness distribution. Because the disk is not infinitely thin, we randomly chose slight offsets from the z-coordinate computed from the precession and inclination angles. The size of the offset depends on a disk aspect ratio $k(r) = h/r$, where $h(r)$ is the disk thickness as a function of radius. We assumed the disk aspect ratio follows a power-law form, $k(r) = k_{50}(r/50'')^{\beta_z}$. The intensity of the emission contributed at each point was then computed assuming that the disk volume emissivity integrated through the disk vertically is a power-law function of radius, $\epsilon(r) \propto r^{-\beta_e}$. We also allowed an inner gap in the radial surface brightness profile, $r_{\rm gap}$. The contribution from the active nucleus and the $\sim$100 pc circumnuclear disk are not taken into account in our model, so by a gap we mean a deficit within $r_{\rm gap}$ and that of the circumnuclear disk at $\sim 6''$.

A model intensity image computed as described above is shown in Figure 4, along with the 8.0 μm IRAC image of the galaxy. The numerical parameters of this model are summarized in Table 1. The angle precession angular functions, $\alpha(r)$, are shown in Figure 5*a*. The precession angle used previously by Quillen et al. (1993) to match the near-infrared morphology is shown as a dotted line in this figure. *Spitzer* improves our ability to study the outer parts of the disk relative to previous ones using the old ^{12}CO(2–1) spectra and near-infrared images. Thus, there are some differences in the precession angle, $\alpha(r)$, between our old model and our newer one, as shown in Figure 5. To better match the morphology in the outer parts of the disk, we allowed the disk to twist further (to a higher value of α) before decreasing at larger radius.

TABLE 1
Model Parameters

Description	Parameter	Value
Galaxy Principal Axis		
PA on sky (deg)	χ	20
Tilt (deg)	ϑ	75
Dust Intensity		
Dust emissivity index	β_e	4.0
Aspect ratio	k_{50}	0.1
Aspect ratio index	β_k	0.9
Radius of inner hole (arcsec)	$r_{\rm gap}$	50

Notes.—The precession angle for this model, $\alpha(r)$, is a spline function that interpolates between 10 points (radius in units of arcseconds, α in units of degrees): (0.2, 180), (36.0, 210), (57, 270), (80, 345), (89, 375), (100, 400), (135, 380), (155, 345), (240, 280), and (400, 240). The inclination angle $\omega(r)$ is a spline function that interpolates between the following points: (0.2, 25), (100, 20), (260, 8), and (400, 8).

Our model predicts that the disk alternates between having the southern side and northern side nearest, with folds both above and below the nucleus. Figure 6*b* shows the distance on the sky north or south of the nucleus in the model disk as a function of distance along the line of sight. The features in the mid-infrared images arise from folds on either side of the nucleus; however, only folds nearer the observer correspond to features seen in extinction. The near-infrared images show a strong dust absorption feature to the southwest of the nucleus, corresponding to an inner fold, and a weaker feature north of the nucleus, corresponding to an outer fold (Quillen et al. 1993). The inner fold is seen as the parallelogram in the mid-infrared images and the outer fold as the oval (see Fig. 3). In Figure 6*a* we show the rings comprising our warp model, projected on the sky. The nearer semicircle of each ring is shown in black, whereas the more distant semicircle is shown in gray. The disk at $r \sim 60''$ is nearest the observer on the southeast side. This region corresponds to a fold in the disk that is seen in the near-infrared color map, $10''$ to the southeast of the nucleus (see Fig. 3). At $r \gtrsim 100''$ the northern side of the disk is again nearest the observer. This corresponds to the northern dust lane seen in the optical images and the near-infrared color map about $45''$ north of the nucleus.

3.1. *Comparison to Previous Studies on the Geometry of the Warped Disk*

Figures 7*a* and 7*b*, show the inclination and position angles as a function of radius with respect to the viewer, compared to those found by Nicholson et al. (1992) from kinematic fits to the Hα velocity field (see their Figs. 9*a* and 9*c*). Nicholson et al. (1992) adopted a distance of 3 Mpc to Cen A; we have corrected for this 15% difference by rescaling their distances. We see from Figure 7 that the position angles of their tilted ring fit are quite similar to those predicted by our model.

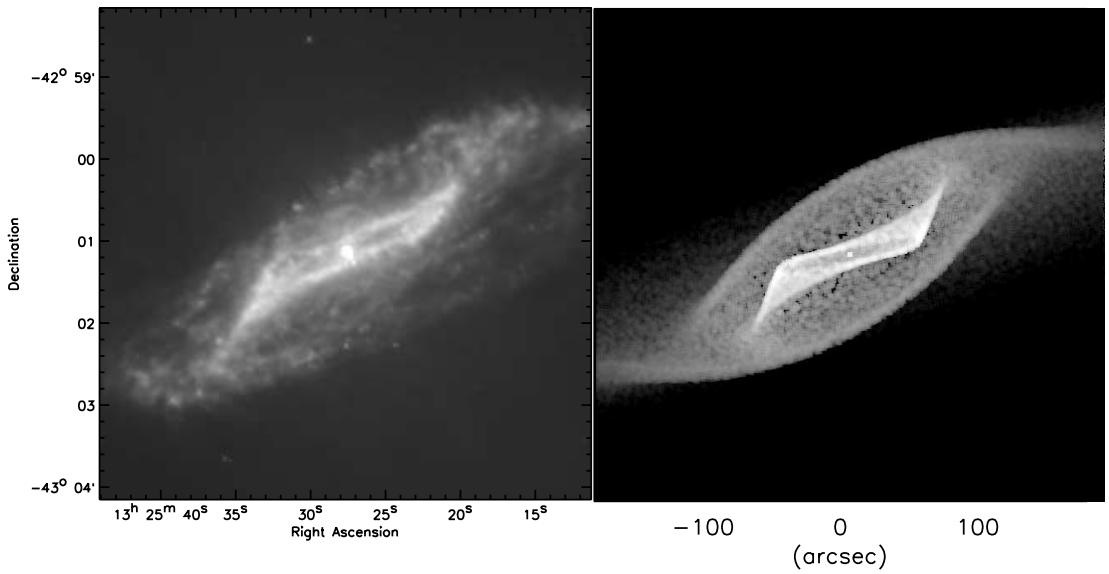

FIG. 4.—*Left:* IRAC 8.0 μm image. *Right:* Model for the warped disk with parameters given in Table 1. Note: 1′ approximately equals 1 kpc.

The warp shape originally designed to match the velocity field in molecular gas (Quillen et al. 1992) resembled that which matched the Hα velocity field by Nicholson et al. (1992). Both models included an inclined disk that tilted so that gas rings at different radii alternated between being retrograde and prograde with respect to the observer. This was also a characteristic of the high-inclination warp model for NGC 4753 by Steiman-Cameron et al. (1992). The tilted ring fitted by Nicholson et al. (1992) to the velocity field did not specify which side of each ring was closest to the viewer. However, Bland (1986), Bland et al. (1987), Nicholson et al. (1992), and Quillen et al. (1993) used the visible and near-infrared images to break this degeneracy. The disk is tilted so that it is nearer the viewer on the southern side for intermediate radii, accounting for the southern edge of the dust lane seen in optical images, and nearer the viewer on the northern side at largest radii to account for the northern dust lane seen in the optical and near-infrared images. These flips in orientation can be seen from Figure 7*b*. They occur where the inclination with respect to the viewer crosses 90°, at which point the disk is edge-on.

The model by Quillen et al. (1993) had a somewhat lower inclination for the galaxy principal axis, $\vartheta = 65°$, instead of the value of 75° used here. Their model also had a higher disk inclination with respect to the galaxy principal axis at smaller radii. There is redundancy in the model between the inclination of the disk with respect to the galaxy axis, $\omega(r)$, and the tilt of the galaxy principal axis, ϑ. The maximum and minimum ring inclinations correspond to values set by $\vartheta \pm \omega$ (see discussion by Quillen et al. 1992). To exhibit the parallelogram shape, the disk inclination with respect to the viewer must go above and below 90°, causing folds in the disk. This restricts the models to a range of values $\vartheta + \omega \sim 100°$.

Here we find a somewhat better match (see Fig. 8) to the mid-infrared images with a model that has decreasing inclination (with respect to our estimated galaxy principal axis) at larger radii. However, this decrease may be spurious. The numerical procedure sets the number of disk points per unit area on the disk. To resolve structure in the inner disk, a large number of points per unit area are required, and such a model cannot be integrated to large radius. By accounting for every observed feature, we may have achieved a better morphology match with a model that has exaggerated variations in the ring angles. In other words, the angular variations may have been compressed into smaller radii than they should have been.

To be more certain of the orientation of the outer disk, better kinematic constraints on this outer disk are needed. By specifying a choice for the principal axis of the galaxy, we have chosen to describe the geometry of the warped disk with respect to a particular axis. This choice helped Quillen et al. (1993) compare the shape of the disk to the predictions of simple merger and precessing ring models. However, it is not necessarily significant that the disk inclination as measured with respect to our assumed galaxy axis varies slowly with radius. An additional complexity not considered with our choice of projection angles is that the galaxy may be triaxial or may significantly vary in shape and orientation with radius (e.g., as considered by Arnaboldi & Sparke 1994). The galaxy is in the process of dynamic relaxation following the merger. Analytical models or one-dimensional integrations fail to capture the complexity of more detailed numerical simulations, particularly for near-equal mass mergers (e.g., Mihos 1999; Mihos & Hernquist 1996). Imaging and kinematic studies of the outer galaxy suggest that these additional degrees of freedom are important (Malin et al. 1983; Schiminovich et al. 1994; Hui et al. 1995; Peng et al. 2002).

3.2. *Comparison to the Dynamical Warp Models*

The model precession angle $\alpha(r)$ reaches a maximum at $r \sim 100''$, decreasing at both larger and smaller radii (see Fig. 5). This implies that the corrugated disk is twisted in one direction for $r \lesssim 100''$ and in the opposite direction for $r \gtrsim 100''$. Since the near-infrared morphology depends on which side of each ring is closer to the observer, and our model is similar to that used to match the near-infrared images (also see discussion by Bland et al. 1987; Nicholson et al. 1992), this peculiar change in the handedness of the twist is likely to be real.

The precession rate of a gas ring inclined with respect to the underlying galaxy undergoing circular motion is proportional to the ellipticity of the galactic gravitational potential and the angular rotation rate of the ring (e.g., Tubbs 1980; Sparke 1984). If the self-gravity of the ring is important, then it too can affect the precession rate (Sparke 1986; Arnaboldi & Sparke 1994; Sparke 1996). The direction of precession depends on the orientation of the ring and galaxy (whether a polar ring or not) and whether the

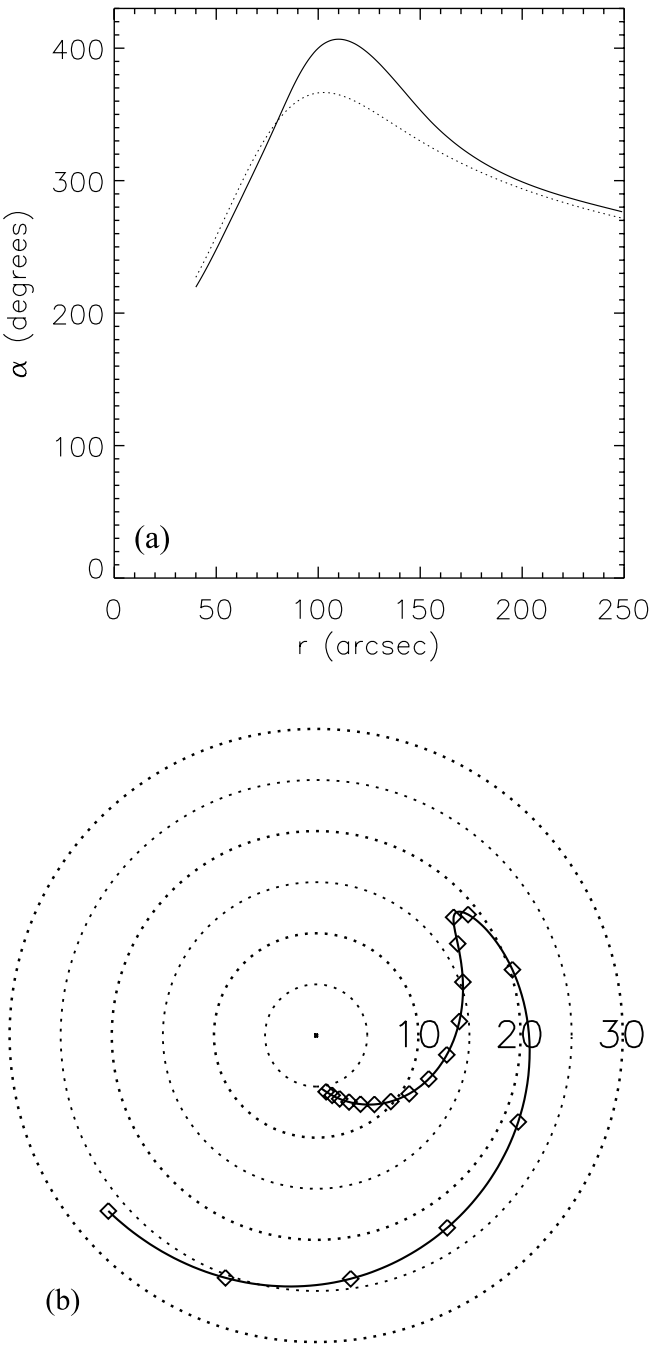

FIG. 5.—(*a*) Model precession angle. The solid line shows the precession angle, $\alpha(r)$, as a function of radius, that was used to make the model shown in Fig. 4. For comparison, we show as a dotted line the precession angle used for the previous model by Quillen et al. (1993) (based on the near-infrared imaging). These models should be approximately consistent with the CO velocity field by Quillen et al. (1992) and the Hα velocity field by Nicholson et al. (1992). (*b*) TIPLON or polar plot showing the angles α and ω. On this plot the inclination angle or tilt, ω, is plotted radially, whereas the precession angle α determines the polar coordinate on the plot. Each dotted circle corresponds to a value for ω, and circles are labeled in degrees along the $\alpha = 0$ axis. The outermost point corresponds to the disk orientation at an inner radius of 40″. Points are shown at radii separated by 10″. Note the change in direction of the twist discussed in § 3.1.

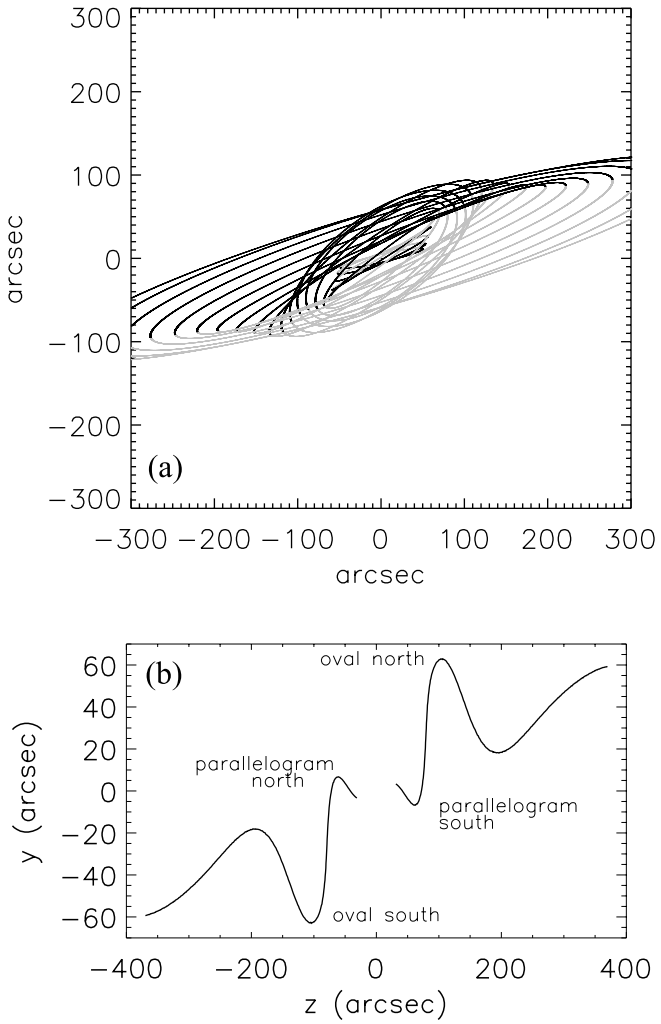

FIG. 6.—Rings for the warped disk model displayed in Fig. 4. The semicircle of each ring nearest the observer is shown in black, and the more distant semicircle is shown in gray. At near-infrared and visible wavelengths, dust nearer the observer absorbs more background galactic starlight than does dust more distant from the observer. The inner fold corresponds to the extinction feature southeast of the nucleus seen in the *J*-band/*H*-band color map (see Fig. 3). The outer fold seen here corresponds to the extinction feature north of the nucleus that is the northern edge of the dust lane prominent in visible images of the galaxy. Regions where rings are close together correspond to regions of higher surface brightness in the mid-infrared images. Although the nearer side can cause deeper extinction features in the near-infrared images, both sides of the disk cause emission features in the mid-infrared images. Note: 1′ approximately equals 1 kpc. (*b*) Disk position along the north-south axis (*y*-axis) as a function of distance in the direction along the line of sight (*z*-axis). Folds in the disk are labeled according to the feature names (see Figs. 3*a* and 3*c*). Here a positive *z*-value corresponds to the nearer side of the disk. Folds on the nearer side correspond to absorption features seen in the 2MASS images (see Figs. 3*a* and 3*b*). [*See the electronic edition of the Journal for a color version of this figure.*]

galaxy is prolate or oblate. Most models assume that, following a merger, the gas and dust are distributed in a plane that is misaligned with the principal axes of the galaxy. To be consistent with the direction of the twist in the outer parts of Cen A [decreasing $\alpha(r)$ at $r \gtrsim 100''$], the galaxy can either be prolate and the ring would be located near the equatorial plane (Quillen et al. 1993), or the galaxy can be oblate and the ring would be nearly polar (Sparke 1996).

The reversal in the sign of the slope ($d\alpha/dr$) is unlikely to be caused solely by the shape of the rotation curve. The predicted rotation curve of Cen A increases at smaller radius, all the way to a radius of 10″ (see Fig. 13 by Marconi et al. 2006). Consequently the angular rotation rate should increase as the radius decreases, nearly all the way to the galaxy center. The rotation curves used by Quillen et al. (1993) and Sparke (1996) were nearly solid-body at small radii, and so they underestimated the angular precession rate at small radii (within ∼1.′5 of the nucleus).

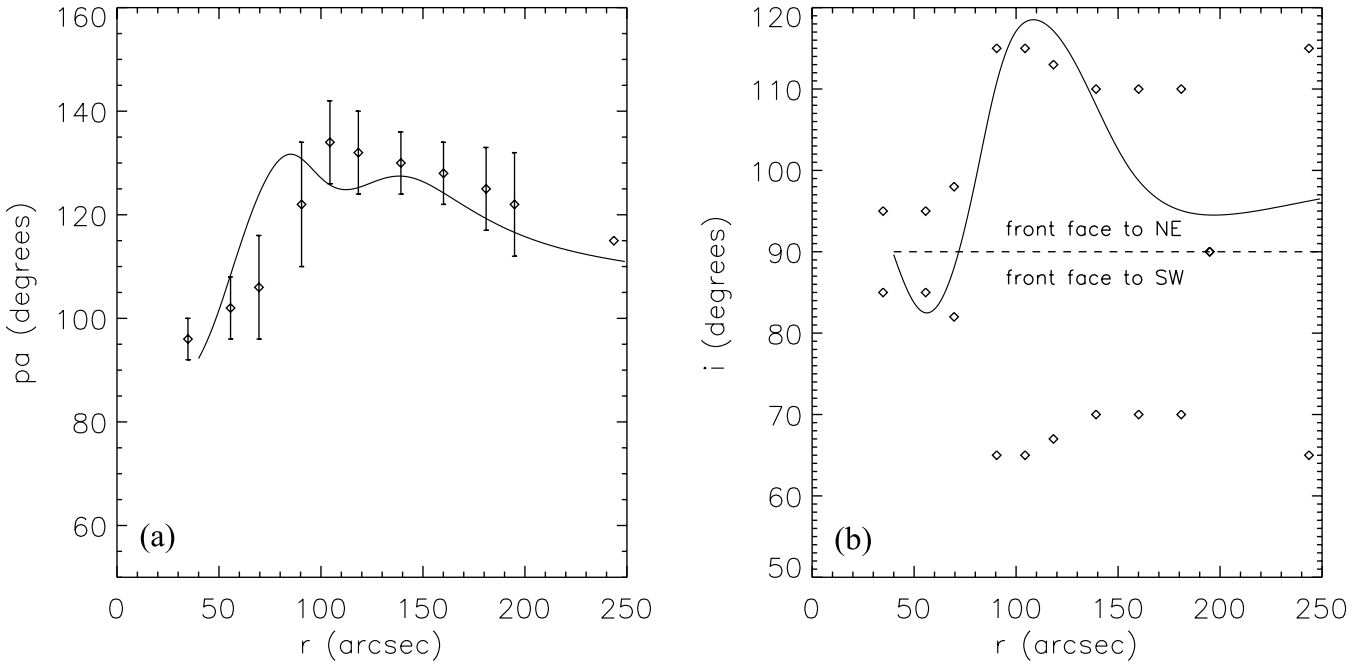

FIG. 7.— (*a*) Position angle of each ring on the sky (counterclockwise from north). These angles are compared with those estimated from tilted ring fits from the Hα velocity field by Nicholson et al. (1992), which are shown as diamonds. These points were taken from their Fig. 9*a*. (*b*) Inclination angle of each ring with respect to the viewer for the model shown in the previous figures. The inclination of an edge-on disk is shown as a dashed line at 90°. Rings with inclinations above 90° are oriented with their nearest points to the northeast of the nucleus, and those with inclinations below 90° have their nearest points to the southwest of the nucleus. These angles are also compared with those from the Hα velocity field (*diamonds*). Bland et al. (1987) and Nicholson et al. (1992) inferred that at $r \lesssim 60''$ the front face of the disk is oriented to the southwest of the nucleus, and vice versa for $r \gtrsim 60''$ (also see Sparke 1996).

The reversal in the sign of the slope ($d\alpha/dr$) could be due to a drop in the galaxy eccentricity (exploited by both Quillen et al. 1993 and Sparke 1996) that would reduce the precession rate at small radii. To account for the change in the slope of α at $r \sim 100''$, Quillen et al. (1993) assumed a sharp cutoff in the ellipticity of the gravitational potential of the galaxy as a function of radius. For $r < 80''$, the potential ellipticity was much reduced in the model by Quillen et al. (1993) compared to that outside it. The galaxy isophotes are best viewed in the short-wavelength 3.6 μm IRAC image (Fig. 9), where the stellar light contributes to the flux and the extinction and emission from dust is minimized compared to that at shorter wavelengths.

We first examine the isophotes at 3.6 μm to search for evidence of the large-scale stellar bar proposed by Mirabel et al. (1999). If such a bar were responsible for the parallelogram shape in the mid-infrared images, the bar would be viewed at intermediate inclinations (not edge-on) and so should be evident in the isophote shapes. Along the major axis of a bar, the surface profile should be flattened near the ends of the bar. However, a surface brightness profile with shoulders is not seen in Cen A.

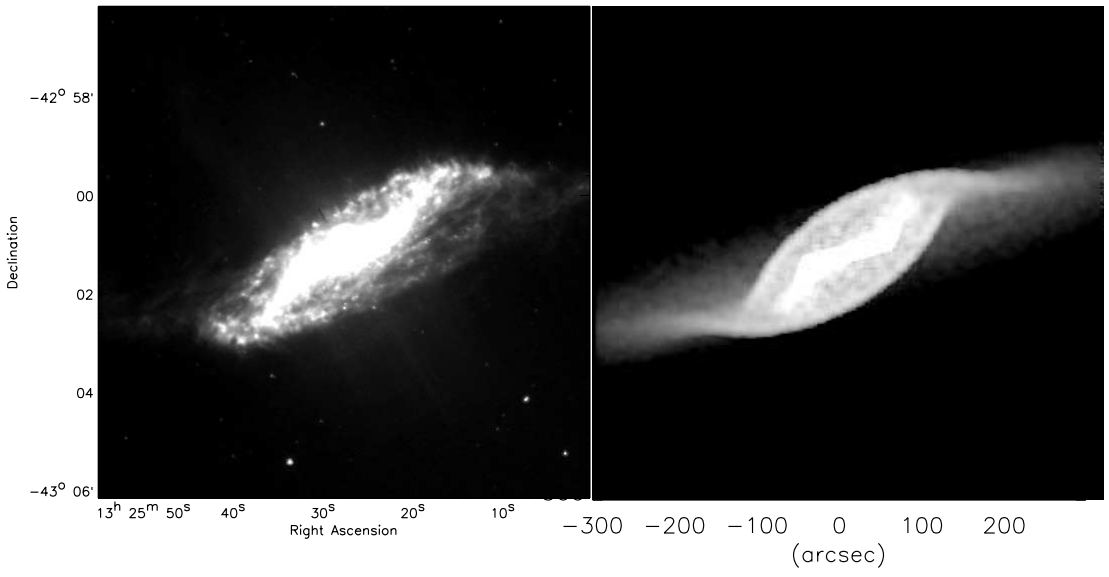

FIG. 8.—Similar to Fig. 4, but shown on a larger scale.

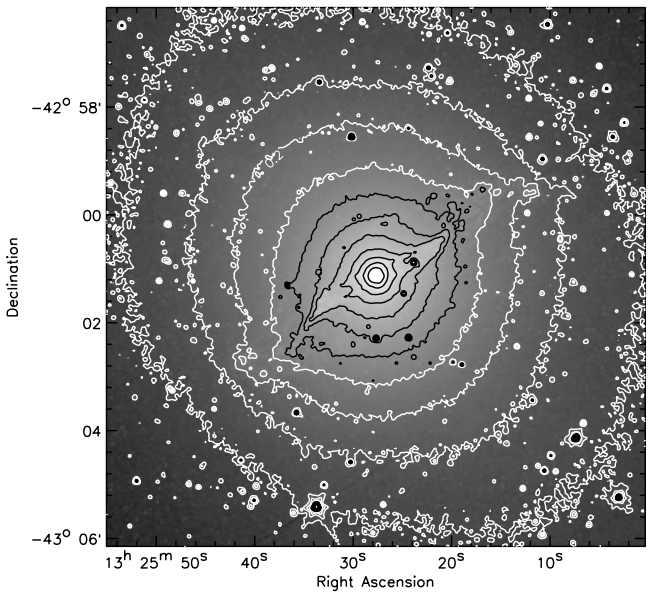

FIG. 9.—IRAC band 1 (3.6 μm) image, shown with isophotal contours. The lowest contour is at 0.63 MJy sr^{-1}. The contours are separated by 0.5 mag or a factor of 1.585. The galaxy is more highly elliptical at larger radii.

A change in the position angle of the isophotes is expected within a bar compared to the angle outside it. However, there is no sharp change in the position angle of the isophotes. We conclude that there is no evidence for a large-scale, few kpc sized, stellar bar at the heart of Cen A.

The galaxy isophotal ellipticity does decrease in the inner regions. By fitting contours to the 3.6 μm image outside the emitting disk, we measured a galaxy isophotal ellipticity for the stellar distribution ($\epsilon = 1 - b/a$, where b and a are the semiminor and semimajor axes) of $\epsilon \sim 0.1$ at $r \sim 4'$, $\epsilon \sim 0.05$ at $r \sim 2'$, and $\epsilon \sim 0$ at $r < 1'$. Because the gravitational potential is a convolution of the density profile with a $1/r$ function, the gravitational potential contours are smoother than the associated density distribution. However, the isophotes are likely to be rounder and smoother than the actual density distribution. While the drop in background galaxy ellipticity exploited by Quillen et al. (1993) and Sparke (1996) in their dynamical models is real, it may not be sharp enough to account for the abrupt drop in the precession rate inferred in the central region of the galaxy from the change in the slope of the precession angle α at $r \sim 100''$.

We now consider the role of the mass in the disk. Sparke (1996) showed that the self-gravity of the disk could increase the precession rate and vary the precession axis in the central region. Sparke (1996) only considered the mass in the molecular and atomic gas components. Quillen et al. (1993) noted that there were extensions in the *K*-band isophotes that were not reproduced by the purely absorptive disk model. The *K*-band isophotes are extended at a radius of about 60″ in the 15 mag arcsec^{-2} contour (also see the dereddened contour map in Fig. 9 of Marconi et al. 2006). We can compare the mass in a possible disk gas and stellar component to that in the underlying galaxy. With a circular rotational velocity of 250 km s^{-1}, a total mass of $\sim 10^{10}\ M_\odot$ is enclosed within a radius of 1 kpc. The mass in molecular gas in the same region is a few times $10^8\ M_\odot$ (Phillips et al. 1987, corrected for the difference in the assumed distance). The level of 15 mag arcsec^{-2} in the *K* band corresponds to a surface density of 4500 $M_\odot$ pc^{-2}, assuming a mass-to-light ratio at the *K* band of 0.5 (e.g., Silge et al. 2005). The actual surface density would be $\sim$10 times lower than this, taking into account the mean disk axis ratio on the sky. This surface density can be compared to the estimated surface density of molecular gas, of a few hundred $M_\odot$ pc^{-2}. This suggests that at least an equal mass exists in stars in the disk as in gas.

By comparing the total mass in gas and stars in the disk to that in the underlying spherical component, we estimate that a few percent of the total mass within 1 kpc lies in the disk. The mass in the disk is likely to be a few times larger than that used by Sparke (1996) to account for the disk geometry. We support the finding by Sparke (1996) that the self-gravity in the disk is important and so should significantly affect the disk precession rate. Future modifications of the prolate model should take this into account, as the self-gravity in the disk could change the direction of precession in this region. If the outer disk is prolate, then a reversal in the twist could be due to the self-gravity of the disk in the inner region. If the outer galaxy is oblate, then the ring is polar and the model by Sparke (1996) would account for the reversal in the twist of the disk. Both dynamical models should be updated to include better estimates of the mass in the disk, the galaxy isophotes at 2.2 and 3.6 μm, and an improved rotation curve based on the light distribution.

3.3. *A Gap in the Dusty Disk between Radii of* 6″ *and* 50″

The model that is most similar to the IRAC images (shown in Fig. 4) contains a gap in the dust distribution with an outer radius $r \sim 50''$. We compare the model shown in Figure 4 to a similar one that lacks the deficit in the dust distribution. This model is shown in Figure 10*a*, and it does not match the observed morphology as well as does that containing a gap in the dust distribution. Continuation of the precession angle into the inner region results in an edge-on disk with respect to the viewer at some point within $r = 60''$. This causes the sharp bright linear feature at $r < 60''$ seen in Figure 10*a* that is not exhibited by the IRAC images.

If the disk has a lower inclination with respect to the viewer, the observed surface brightness is reduced. We consider the possibility that the disk precession angle differs in the inner region from that expected from a smooth continuation of our model. To test this possibility, we computed a model that has a flattened (nontwisted) disk at $r \lesssim 60''$. This model is shown in Figure 10*b*. The sharp, bright, inner feature along the east-west direction seen in Figure 10*a* is not evident in Figure 10*b*. However, the morphology of this model also does not display the characteristics of our preferred model shown in Figure 4. In particular, the triangular features to the southeast and northwest of the nucleus that are seen in the near-infrared color maps on the southeast side (Quillen et al. 1993) are not as good a match to those of the IRAC images. To remove the bright inner feature of Figure 10*a*, the precession angle must remain above $\alpha > 270°$. However, the curved triangle edge of emission in the parallelogram is not present if the precession angle does not steeply drop between a radius of 100″ and 50″. We have tried models with both increasing and decreasing precession angles near the nucleus, finding no improved match to the observed morphology. Our best match is the model with an inner gap in the dust distribution. We explored models with a lower but constant surface density within the estimated gap radius of $\sim$50″, and we can exclude those with a surface density in the gap that is above $\frac{1}{5}$ of that at the outer gap edge.

Previous studies have discussed the possibility of a deficit in the gas distribution in the same region where we find a deficit in the dust distribution. At 100–200 pc from the nucleus, there is a circumnuclear molecular disk that has been studied in molecular line emission (Israel et al. 1990, 1991). A deficit in the ionized

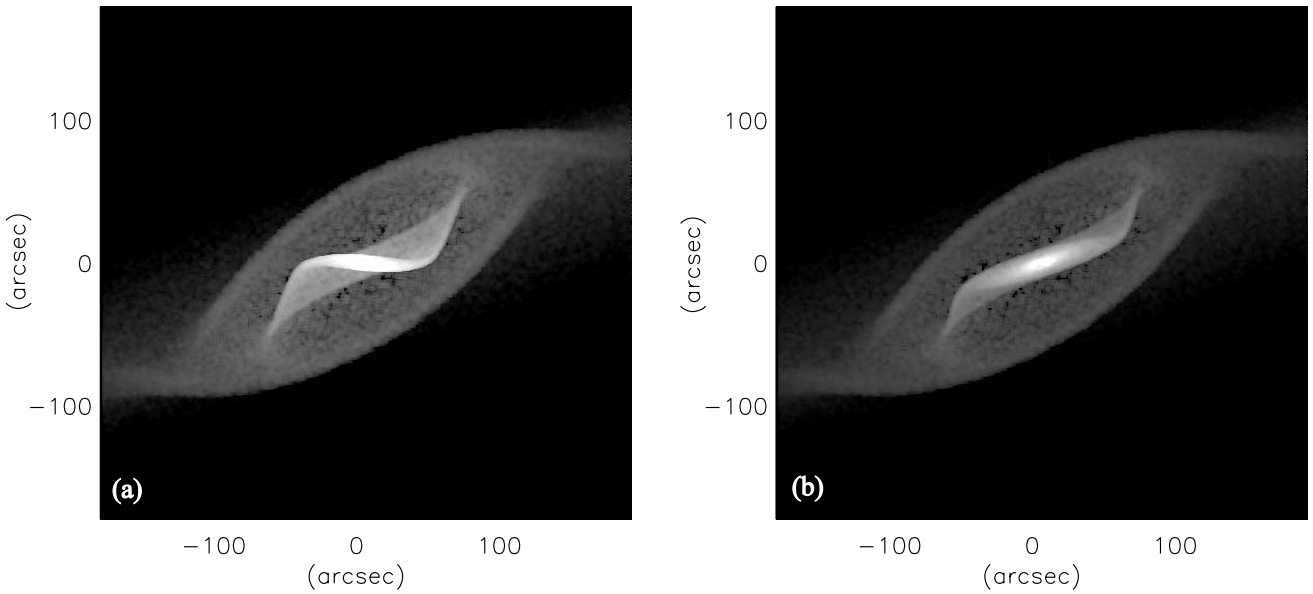

FIG. 10.—(*a*) Similar to the model shown in Fig. 4, but with no deficit in the dust distribution within r_{gap}. (*b*) Similar to the model shown in Fig. 4, but the precession angle $\alpha(r)$ remains above 270° for $r < 50''$. The IRAC images are best matched with a model that contains a deficit in the dust distribution within $r \sim 50''$.

gas distribution outside the circumnuclear disk was seen in the Paα kinematics by Marconi et al. (2001). In Paα, the circumnuclear disk at a radius of $r \sim 6''$ is seen, and so is emission at significantly lower velocities (hence, inferred larger radii) and significantly higher velocities (within the sphere of influence of the massive black hole). However, Paα emission is lacking at intermediate radii and velocities. This lack of emission would be expected if there were a deficit of gaseous material between the radii of $\sim 6''$ (set by the estimated outer radius of the circumnuclear disk; Schreier et al. 1996; Marconi et al. 2000, 2001) and $50''$ (estimated from our model).

The rotation curve previously fitted to the CO and Hα kinematics rose linearly (solid body) within a radius of $1'$ of the nucleus (Nicholson et al. 1992; Quillen et al. 1992). Because an edge-on gas ring appears linear on a position-velocity diagram, a gas disk with an inner hole can mimic or be confused with a gas disk extending all the way to the nucleus in a galaxy with a linearly rising rotation curve. Nicholson et al. (1992) showed that there was a discrepancy between their measured rotation curve and that expected from a $r^{1/4}$ or de Vaucouleurs law. They listed a possible hole in the H II region distribution as a possible cause for this discrepancy. A linearly rising rotation curve within a radius of $1'$ of the nucleus is not consistent with the *K*-band surface brightness profile (see the rotation curve predicted in Fig. 13 by Marconi et al. 2006). The apparent region of solid-body rotation need not be accounted for with a galactic bar, as proposed by Mirabel et al. (1999), and can be better explained by a gap in the gas and dust distribution.

4. SUMMARY AND DISCUSSION

By integrating the light through an emitting, optically thin, dusty, and warped disk, we have successfully matched the morphology of Centaurus A seen in mid-infrared IRAC images. We confirm previous proposals that the disk morphology is well explained by a warped disk (Bland 1986; Bland et al. 1987; Nicholson et al. 1992; Quillen et al. 1993; Leeuw et al. 2002) rather than a barred one (Mirabel et al. 1999). The disk is nearly edge-on with respect to the viewer, but tilts so that folds appear above and below the galaxy equator. There is a fold south of the nucleus at a radius $r \sim 60''$ that is responsible for the high extinction seen in near-infrared images, and a fold north of the nucleus at larger radii that is responsible for the northern edge of the dust lane seen in optical images. Extinction features seen in the near-infrared extinction map correspond to folds in the disk that are located nearer the observer and so absorb more background stellar light from the galaxy. In the mid-infrared, however, folds on both the near and far sides of the galaxy correspond to bright emission features. The inner folds account for the parallelogram shape, while the outer folds account for the northern edge of the dust lane seen in optical images and a fainter oval of emission seen outside the parallelogram in the IRAC images.

The disk geometry we use to match the mid-infrared morphology is similar to that found previously by Quillen et al. (1993) and is also similar to that required to fit the CO and Hα velocity field (Bland et al. 1987; Nicholson et al. 1992; Quillen et al. 1992). The geometric warp models by Nicholson et al. (1992) and Quillen et al. (1993) have been predictive; they provide good matches to the mid-infrared morphology. CO, Hα spectra, and near-infrared imaging were not sensitive enough to provide tight kinematic constraints on the outer disk. The *Spitzer* data have allowed us to extend the model past $r \sim 100''$, compared to previous models, and see closer in to the nucleus, where the extinction is high at shorter wavelengths. Better constraints on the disk geometry will be achieved in the future by fitting observations at more than one wavelength. For example, modern high-resolution kinematic observations that are fitted along with the *Spitzer* data using the same model would allow much stronger constraints on the disk geometry and gas and dust distribution than the slight modification to previous geometric models that we have used here.

The warp disk model suggests that there is a gap in the dusty disk at $6'' \lesssim r \lesssim 50''$. A gap exists in the same region in the gas distribution. Marconi et al. (2001) saw a deficit of Paα emission near the nucleus at intermediate velocities. Nicholson et al. (1992) suggested that the discrepancy between the measured linearly rising rotation curve within a radius of $60''$ might be explained by a hole in the ionized gas distribution. It is not easy to determine if there is a gap in the dust distribution, since the infrared surface brightness depends on the inclination of the disk and the disk is

highly corrugated. If the disk twists to lower inclinations (closer to face-on) at small radii, it would have a lower surface brightness near the nucleus. We have explored models with smoothly varying radial surface brightness distributions and smoothly varying precession and inclination angles. We find that only models with a deficit of dust interior to $\sim 50''$ match the mid-infrared images. We exclude models that have more than $\sim\frac{1}{5}$ of the surface density within $r = 50''$ as what we find at that radius. We conclude that there is a gap in the gas and dust distribution between 0.1 and 0.8 kpc from the nucleus. The inner radius of the gap we have taken from studies of the circumnuclear disk (Marconi et al. 2001; Israel et al. 1991), and the outer radius is estimated from our model.

It is interesting that only the region between the circumnuclear disk (100–200 pc) and ~0.8 kpc has been depleted of gas and dust. While we find no evidence for a large-scale stellar bar in Cen A, a dense gas disk could have exhibited dynamical instabilities depositing gas into the circumnuclear disk (e.g., Shlosman et al. 1989). Energetic star formation or activity associated with the black hole can deplete and evacuate the central region of a galaxy (e.g., Springel et al. 2005; Veilleux et al. 2005), although it is not clear how a circumnuclear disk would be protected from or reformed following this activity. Nearby galaxies exhibit evacuated central regions or circumnuclear rings. For example, the Circinus galaxy has a ~500 pc radius molecular ring (Curran et al. 1998) and contains a Seyfert nucleus. M82 contains a 1 kpc radius circumnuclear molecular ring; however, a previous epoch of star formation has occurred within this ring (e.g., Förster Schreiber et al. 2003). Future observational studies may differentiate between the role of star formation, dynamical instabilities, and nuclear activity in disrupting the gas and dusty disk in Cen A.

The best matching geometric warp model requires a change in the slope of the precession angle at a radius of about $r \sim 100''$. Two previous models account for this twist. Quillen et al. (1993) used a model in which the galaxy was prolate in its outer region and the galaxy ellipticity abruptly dropped to zero within $r \sim 80''$. However, this abrupt drop is not consistent with the isophote shapes at 3.6 μm. A prolate model (with the advantage of a relatively short timescale) might account for the disk geometry if modified to include the self-gravity of the disk. The polar ring model by Sparke (1996) naturally accounts for the reversal, but requires a longer timescale to operate. These dynamical models could be updated to use a more accurate mass distribution and rotation curve. Improvements to these models may lead to better understanding of the galaxy merger that created Cen A's peculiar morphology, as well as the merger's role in feeding the active galactic nucleus.

We thank Joss Bland-Hawthorn, Varoujan Gorjian, and Vassilis Charmandaris for helpful comments and suggestions. A. C. Q. thanks the Research School of Astronomy and Astrophysics of the Australian National University and Mount Stromlo Observatory for hospitality and support during the spring of 2005. Support for this work was in part provided by National Science Foundation grant AST 04-06823 and by the National Aeronautics and Space Administration under grant NNG04GM12G issued through the Origins of Solar Systems Program. We acknowledge support by award HST-GO-10173-09.A through the Space Telescope Science Institute. This work is based on observations made with the *Spitzer Space Telescope*, operated by the Jet Propulsion Laboratory, California Institute of Technology, under NASA contract 1407.

REFERENCES

Arnaboldi, M., & Sparke, L. S. 1994, AJ, 107, 958
Baade, W., & Minkowski, R. 1954, ApJ, 119, 215
Bland, J. 1986, Ph.D. thesis, Univ. Sussex
Bland, J., Taylor, K., & Atherton, P. D. 1987, MNRAS, 228, 595
Charmandaris, V., Combes, F., & van der Hulst, J. M. 2000, A&A, 356, L1
Curran, S. J., Johansson, L. E. B., Rydbeck, G., & Booth, R. S. 1998, A&A, 338, 863
Fazio, G. G., et al. 2004, ApJS, 154, 10
Förster Schreiber, N. M., Genzel, R., Lutz, D., & Sternberg, A. 2003, ApJ, 599, 193
Haynes, R. F., Cannon, R. D., & Ekers, R. D. 1983, Proc. Astron. Soc. Australia, 5, 241
Hernquist, L., & Quinn, P. J. 1988, ApJ, 331, 682
Hui, X., Ford, H. C., Freeman, K. C., & Dopita, M. A. 1995, ApJ, 449, 592
Israel, F. P. 1998, A&A Rev., 8, 237
Israel, F. P., van Dishoeck, E. F., Baas, F., de Graauw, T., & Phillips, T. G. 1991, A&A, 245, L13
Israel, F. P., van Dishoeck, E. F., Baas, F., Koornneef, J., Black, J. H., & de Graauw, T. 1990, A&A, 227, 342
Jarrett, T. H., Chester, T., Cutri, R., Schneider, S. E., & Huchra, J. P. 2003, AJ, 125, 525
Leeuw, L. L., Hawarden, T. G., Matthews, H. E., Robson, E. I., & Eckart, A. 2002, ApJ, 565, 131
Malin, D. F., Quinn, P. J., & Graham, J. A. 1983, ApJ, 272, L5
Marconi, A., Capetti, A., Axon, D. J., Koekemoer, A., Macchetto, D., & Schreier, E. J. 2001, ApJ, 549, 915
Marconi, A., Pastorini, G., Pacini, F., Axon, D. J., Capetti, A., Macchetto, D., Koekemoer, A. M., & Schreier, E. J. 2006, A&A, 448, 921
Marconi, A., Schreier, E. J., Koekemoer, A., Capetti, A., Axon, D., Macchetto, D., & Caon, N. 2000, ApJ, 528, 276
Mihos, C. 1999, Ap&SS, 266, 195
Mihos, J. C., & Hernquist, L. 1996, ApJ, 464, 641
Mirabel, I. F., et al. 1999, A&A, 341, 667
Nicholson, R. A., Bland-Hawthorn, J., & Taylor, K. 1992, ApJ, 387, 503
Peng, E. W., Ford, H. C., Freeman, K. C., & White, R. L. 2002, AJ, 124, 3144
Phillips, T. G., et al. 1987, ApJ, 322, L73
Quillen, A. C., de Zeeuw, P. T., Phinney, E. S., & Phillips, T. G. 1992, ApJ, 391, 121
Quillen, A. C., Graham, J. R., & Frogel, J. A. 1993, ApJ, 412, 550
Schiminovich, D., van Gorkom, J. H., van der Hulst, J. M., & Kasow, S. 1994, ApJ, 423, L101
Schreier, E. J., Capetti, A., Macchetto, F., Sparks, W. B., & Ford, H. J. 1996, ApJ, 459, 535
Shlosman, I., Frank, J., & Begelman, M. C. 1989, Nature, 338, 45
Silge, J. D., Gebhardt, K., Bergmann, M., & Richstone, D. 2005, AJ, 130, 406
Sparke, L. S. 1984, MNRAS, 211, 911
———. 1986, MNRAS, 219, 657
———. 1996, ApJ, 473, 810
Springel, V., Di Matteo, T., & Hernquist, L. 2005, MNRAS, 361, 776
Steiman-Cameron, T. Y., Kormendy, J., & Durisen, R. H. 1992, AJ, 104, 1339
Tubbs, A. D. 1980, ApJ, 241, 969
Veilleux, S., Cecil, G., & Bland-Hawthorn, J. 2005, ARA&A, 43, 769